Control of Void Formation in Adhesively Bonded Joints in the Presence of Filler

Nina S. Dytiuk, Thomas F. Marinis., and Joseph W. Soucy
Draper
555 Technology Square
Cambridge, MA 02139-3563 U.S.
Ph: 617-258-3290
Email: ndytiuk@draper.com

Abstract

Adhesively bonded joints are ubiquitous in electronic assemblies that are used in a wide range of applications, which include automotive, medical, military, space and communications. The steady drive to reduce the size of assemblies in all of these applications, while providing increased functionality, generates a need for adhesive joints of higher strength, improved thermal and electrical conductivity and better dielectric isolation. All of these attributes of adhesive joints are degraded by the presence of voids in them. The quest to minimize voids in bonded structures motivated a previous study of their formation in a solvent cast, die bond epoxy film, which undergoes a liquid phase transition during cure. That work is extended in this study by including the effects of various filler morphologies in the adhesive. Fillers are added to adhesives to facilitate handling of thin sheet formats, control bond line thickness and reduce coefficient of thermal expansion. As such, fillers are selected to be inert with respect to the adhesive chemistry, while being readily wetted by it in the liquid state. Common filler morphologies include woven and molded open meshes, fibers chopped to uniform length, and spheres of uniform or distributed diameters. Void formation is influenced by a number factors, which include wettability of the bonded surfaces, adsorbed water, amount of solvent retained in the film, volume of entrapped air, thermal profile of the cure schedule, and clamping pressure during cure. The presence of fillers in the adhesive adds the additional factors of constrained diffusion paths and increased area for void nucleation. We have changed our approach to modeling the diffusion of volatile species in adhesive joints from a finite difference calculation in a uniform adhesive medium used previously, to a finite element model of a complex diffusion space. The open source program *Gmsh* is used to generate the diffusion space from a set of input parameters. The calculations of concentration profiles and diffusion fluxes of volatile species at the void interface are made using the open source finite element program *elmer*. As done previously, the position of the void interface is updated by integrating the product of time and flux of diffusing species over the area of the interface. The internal pressure of the void is determined by application of the Young-Laplace equation, while Henry's law is used to estimate the concentration of diffusing species adjacent to the void interface. The calculation proceeds for a time equivalent to the integral of the time temperature product required to achieve a 70% cure state of the adhesive, at which point the void interface is immobile. The experimental approach is the same as used previously, with the filled adhesive sandwiched between glass slides and cured on a hot plate while imaged through a microscope. Images are automatically captured and analyzed by using the open source program *imageJ*, which allows us to track the evolution of individual voids as well as the time dependent distribution of the void population. We are working to correlate these experimental results with the predictions of our finite element calculations to allow us to make insightful choices of adhesives and optimize our bonding processes.

Key words

Void, adhesive joint, die bond epoxy film, diffusion, filler

I. Introduction

Adhesive joints in electronic assemblies are used to provide physical attachment of components, conduct heat away from active devices, enable electrical connections, confine fluids in biological and chemical sensors, and enable integration of electronics with larger structures in air frames, energetic devices and wearable systems. As with other aspects of electronic packaging, adhesive joints are becoming smaller, pushing materials closer to their ultimate strength values and reducing the tolerance for defects, such as voids [1]. In a previous paper, we presented a model for shrinkage of voids at a bond interface that was driven by diffusion of volatiles within the void out into adhesive volume [2]. The kinetics of this process were compared to those of the cross-linking reaction during adhesive cure, with the objective of optimizing the cure schedule to achieve the greatest possible void reduction. Time lapse photo-microscopy of voids in a transparent adhesive cured at different temperatures provided good correlation with our model predictions.

In many applications, adhesives are loaded with non-reacting particles for purposes of improving thermal conductivity, increasing fracture toughness, imparting electrical conductivity, or tailoring coefficient of thermal expansion [3],[4]. The addition of filler material can exacerbate the removal of voids in several ways. The introduction of particles increases the surface area for nucleation of voids. Many studies have demonstrated that surface preparation is a key factor for elimination of voids from adhesive bonds [5]. Filler material also decreases the volume of adhesive in which volatiles from the void can dissolve and diffuse away from the interface. Finally, the presence of particles increases the path along which diffusing species must pass to escape from the bond interface.

In this investigation, we apply finite element tools to create three-dimensional models of adhesive bonds that contain a void and particles arranged in different geometric configurations. The flux of diffusing species from the void are computed as a function of time for different volume fractions of filler particles. These results are compared with experimental measurements made on a model adhesive system loaded with different volume fractions of glass spheres. Our objective is to understand how the presence of filler particles impact the kinetics of void reduction during adhesive cure.

II. Modeling

Procedure

The ***elmer*** finite element program package was used to simulate the time dependent change of the concentration field and calculate the flux of diffusing species out of the void interface [6]. The *elmer* solver for thermal flux j and the time rate of temperature change $dT/dt$was used by making a transformation of variables. Starting with the governing differential equations for heat transfer

$$\boldsymbol{j}\ [J\,m^{-2}sec^{-1}] = -k\ [J\,m^{-2}sec^{-1}K^{-1}]\ \boldsymbol{\nabla}\mathrm{T}\ [Km^{-1}] \quad (1)$$

$$C_p\ [JKg^{-1}K^{-1}]\ \rho\ [Kgm^{-3}]\ \frac{\partial T}{\partial t}\ [Ksec^{-1}] = -\boldsymbol{\nabla}\cdot \boldsymbol{j}\ [J\,m^{-3}sec^{-1}] \quad (2)$$

in which k, Cp and p are the thermal conductivity, heat capacity and density of the material, the equation for $dT/dt$is rewritten as the product of a material dependent constant and the Laplassian of the temperature

$$\frac{\partial T}{\partial t}[Ksec^{-1}] = \frac{k[Jm^{-2}sec^{-1}K^{-1}]}{C_p[JKg^{-1}K^{-1}]\rho[Kgm^{-3}]}\nabla^2 T[Km^{-2}]. \quad (3)$$

The constant has the units of diffusivity

$$\frac{\partial T}{\partial t}[Ksec^{-1}] = \frac{k}{C_p\rho}[m^2sec^{-1}]\nabla^2 T[Km^{-2}] \quad (4)$$

so that both side of the equation have units of temperature reciprocal time

$$\frac{\partial T}{\partial t}\ [Ksec^{-1}] = \frac{k}{C_p\rho}\ \nabla^2 T\ [Ksec^{-1}]\,. \quad (5)$$

By normalizing the temperature,

by letting $\eta = T/T_{Ref}$

$$T_{Ref} \equiv highest\ temperature\ in\ system$$

$$\frac{\partial \eta}{\partial t}\ [sec^{-1}] = \frac{k}{C_p\rho}\ \nabla^2\eta\ [sec^{-1}] \quad 6)$$

the differential equation is equivalent to that governing concentration of a diffusing species.

Thus, π represents concentration, which ranges between 0 and 1, and the diffusivity of species is given by the quantity $\frac{k}{C_p\rho}$.

The program *Gmsh* was used to create parameterized, three-dimensional models of voids in an adhesive resin with embedded particles [7]. This paper presents results obtained from four different configurations of cylindrical particles oriented normal to the plane of diffusion. In these pseudo-two dimensional models, the voids are also represented as cylindrical segments with radii that are independent of those of the particles. The geometry generated by the program is dimensionless, so the length scale is set by the units of the diffusivity constant, which for modeling convenience, we have chosen to be (10-5 m)2/sec. The four basic configurations of particles in the diffusion field are shown in Figures 1a through 1d. Only the right-half of the diffusion field, which is assumed to be symmetric about the y-axis, is shown in these images. Half of the void interface is shown in the lower left of the diffusion field. The model shown in Figure 1a contains

one large particle on the right-hand side of the diffusion field. A model that contains two different size particles is shown in Figure 1b. Figure 1c shows a model with eight particles of equal radii that are arranged on a simple cubic lattice structure and a face centered cubic arrangement of seven equal radii particles are shown in Figure 1d.

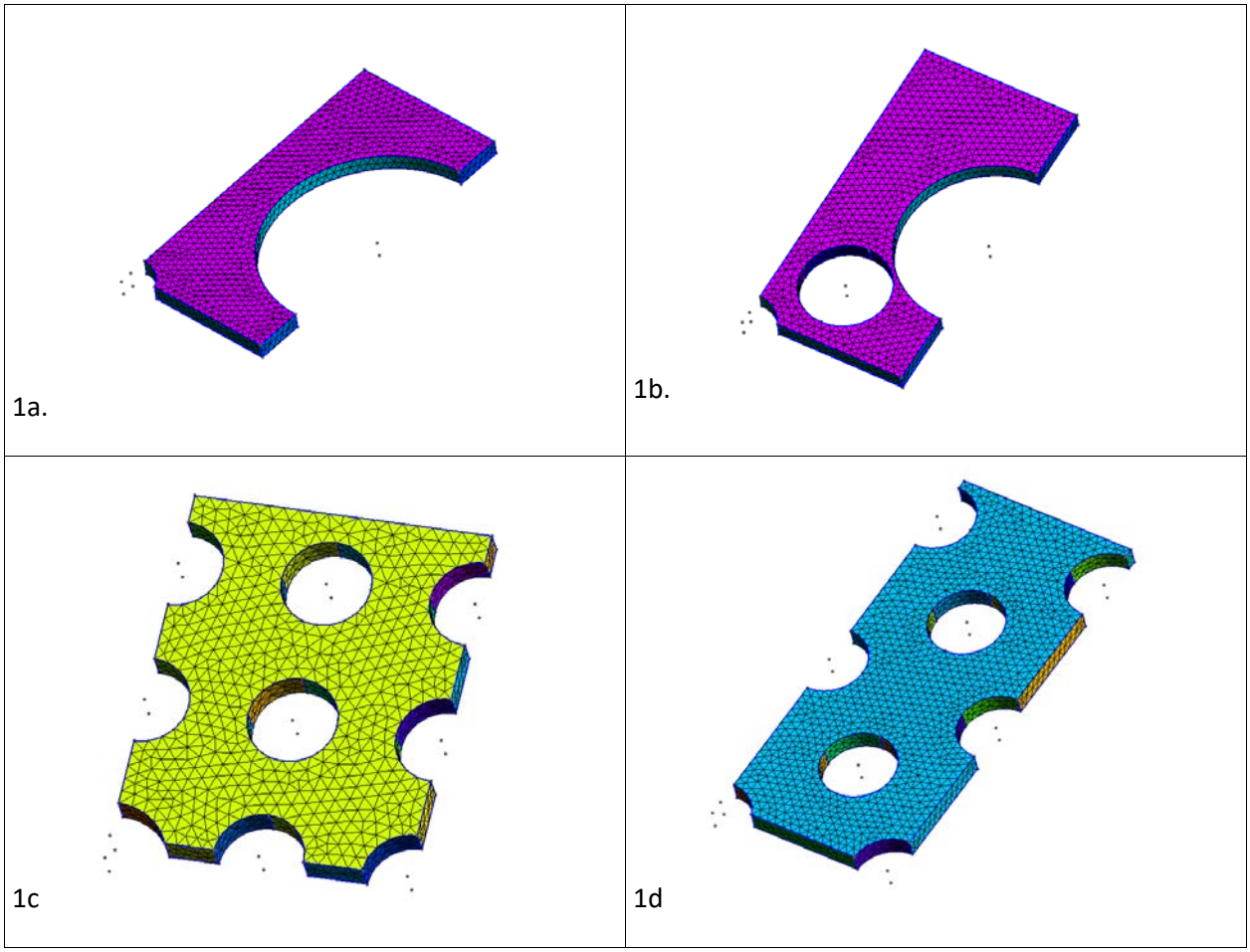

Figure 1. Four arrangements of particles used to model the diffusion of species from a void, that is located in the lower left of each diffusion field. This field is symmetric about the y-axis and cuts the void in half.

It is presumed that at the interface of the void, the adhesive is saturated with the diffusing species, so the concentration is c_{sat} and thus π in equation (6) is set equal to 1.0. There is no diffusion flux across any of sides or particles in the diffusion field. At the face furthest from the void, two different boundary conditions can be imposed. If the adhesive surface is exposed so that the diffusing species can escape, the concentration is fixed at zero. A no flux boundary condition is imposed for modeling adhesive that abuts an impermeable surface.

The model generates concentration maps as a function of time, which are displayed by using the visualization program *paraview* [8]. It also calculates the time dependent flux of species out of the void. Representative images of the time dependent distribution of diffusing species from the four models are shown in Figures 2 through 5. These images are for the case of zero concentration at the far boundary.

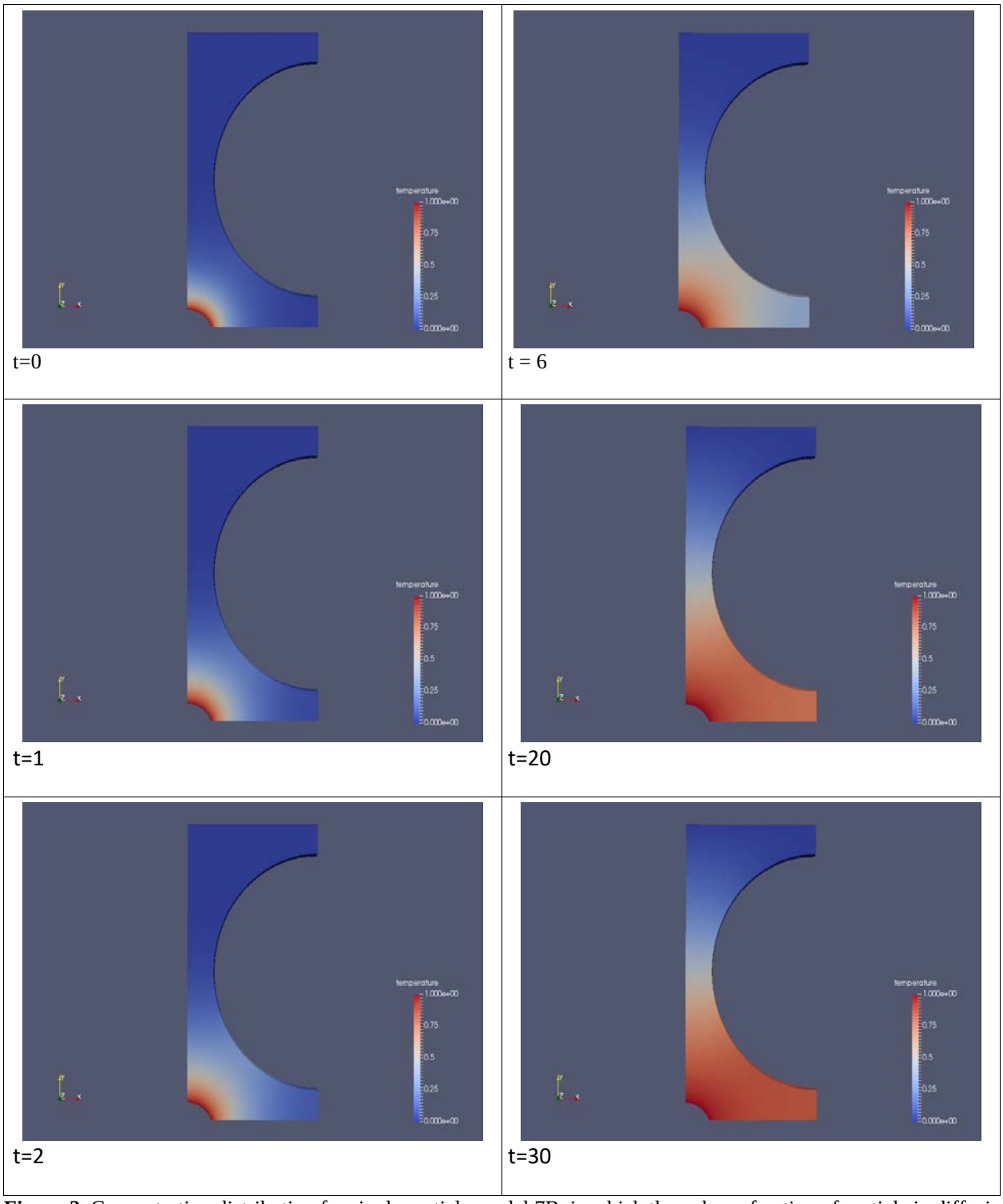

Figure 2. Concentration distribution for single particle model 7B, in which the volume fraction of particle in diffusion field equals 0.50.

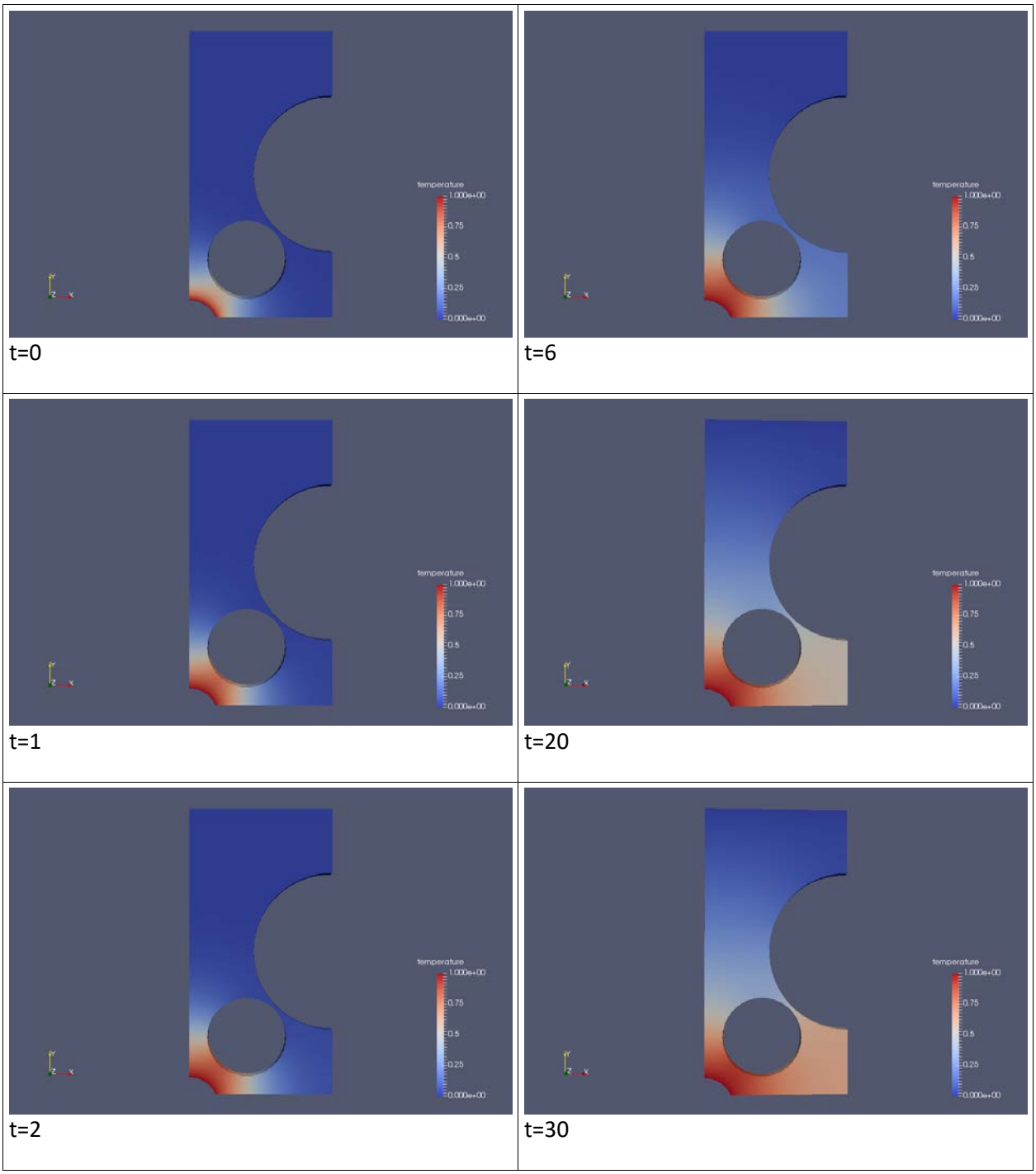

Figure 3. Concentration distribution for two single particle model 8c, in which the volume fraction of particles in diffusion field equals 0.36.

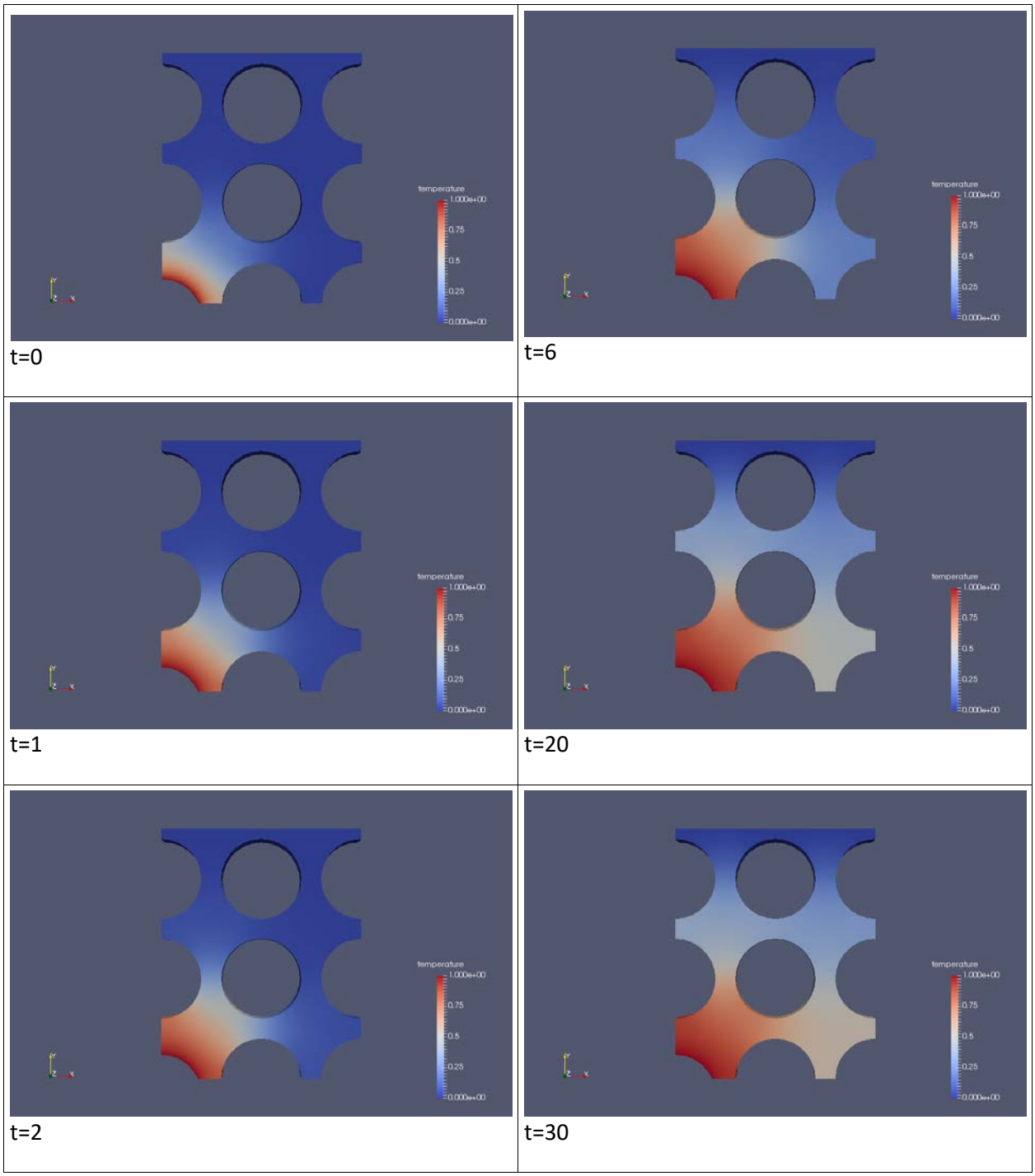

Figure 4. Concentration distribution for model SC2, comprised of eight particles arranged on a simple cubic lattice. Volume fraction of particles in the diffusion field equals 0.48.

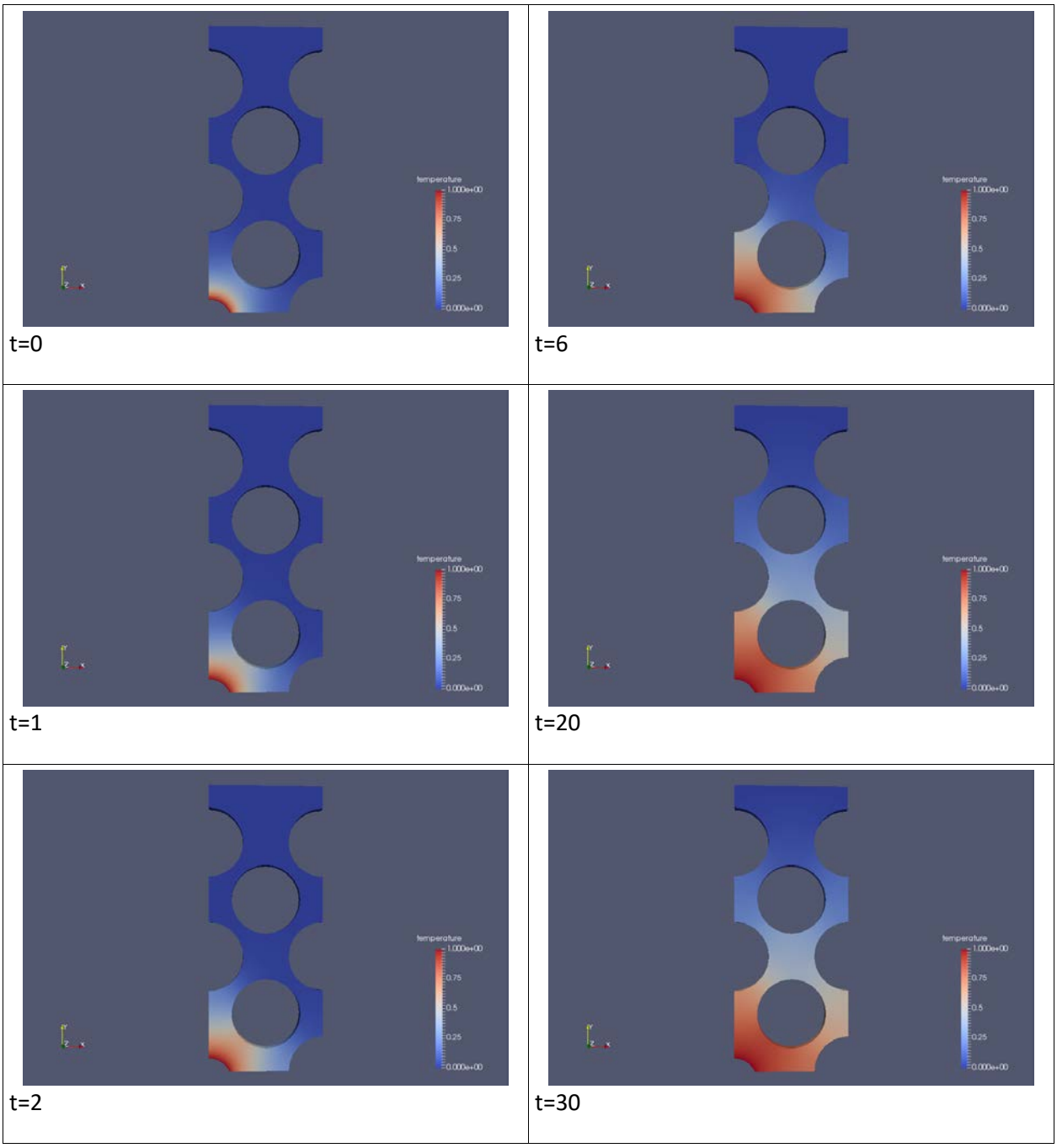

Figure 5. Concentration distribution for model 12, comprised of seven particles arranged on a face centered cubic lattice. Volume fraction of particles in the diffusion field equals 0.48.

The model can address two questions pertaining to the kinetics of void shrinkage in adhesive joints that contain inert filler. The first is, how is the rate of void shrinkage affected by the volume fraction of filler, and second, how dependent is this rate on the distribution of particles within the joint. The rate of void shrinkage is proportional to the flux of diffusing species that cross the void interface. The model calculates this flux at regular time intervals. In Figures 6 through 9, this flux is plotted against time for the single and two particle models, and for the models with particles arrayed on simple cubic and face centered cubic lattices, respectively. In each figure, curves are plotted for

several different volume fractions of particles. The volume fraction, Vf, of particles in each model is calculated as

$$V_f = N_p \pi {r_p}^2 / (X_F Y_F) \quad (7)$$

in which NP is the number of particles of radius rp, in the diffusion field of dimension XF by YF. The value of NP for the for models is

Model	N_P
Single particle	0.5
Two particle	0.75
Simple cubic	4.75
Face centered cubic	4.25

The flux for the single particle model, shown in Figure 6, drops very sharply for all particle volume fractions. After the initial drop, the flux decreases more slowly as time passes, with the rate of decrease strongly affected by the particle volume fraction.

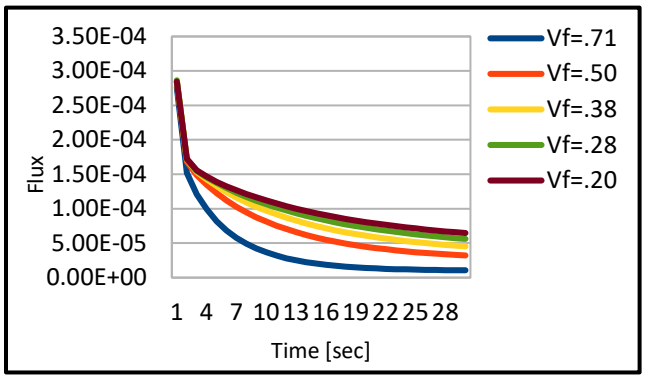

Figure 6. Time dependent flux at the void interface for the single particle model. Curves are shown for particle volume fractions of 0.20, 0.28, 0.38, 0.50, and 0.71

Figure 7 shows the time dependence of the flux for the two particle model. As in the case of the single particle model, the flux drops sharply initially, followed by a period of gradual decrease. Unlike the single particle model, the shape of the curves is not strongly influenced by the volume fraction of filler particles.

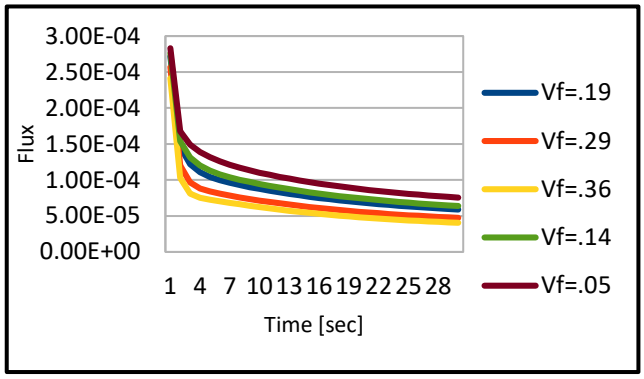

Figure 7. Time dependent flux at the void interface for the two particle model. Curves are shown for particle volume fractions of 0.05, 0.14, 0.19, 0.29, and 0.36.

Computed flux curves for the simple cubic lattice model are shown in Figure 8. An initial sharp drop in flux is followed by a more gradual decline. There is a strong dependence on particle volume fraction. At the highest loading content, the flux changes very little as time progresses.

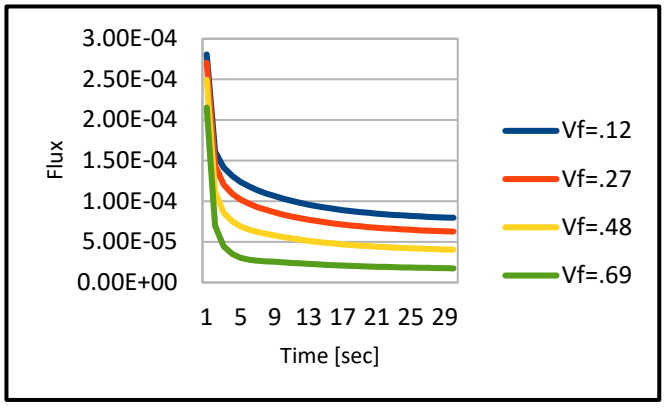

Figure 8. Time dependent flux at the void interface for the simple cubic lattice model. Curves are shown for particle volume fractions of 0.12, 0.27, 0.48, and 0.69

Results for the face centered cubic lattice are shown in Figure 9. The initial sharp decline in flux is followed by a gradual decrease. The shapes of the curves, however, do not change drastically with volume fraction of particles.

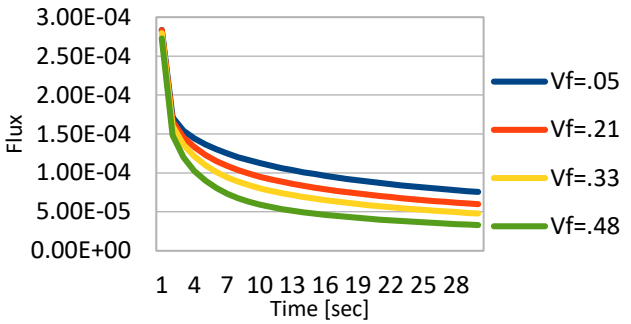

Figure 9. Time dependent flux at the void interface for the face centered cubic lattice model. Curves are shown for particle volume fractions of 0.05, 0.21, 0.33, and 0.48 .

The sharp drop in flux from the void exhibited by all four models is due to the buildup of diffusing species in the immediate vicinity of the void. The scale of this concentration gradient is small compared to the size of the filler particles, which is why it is unaffected by the arrangement or volume fraction of filler particles. In Figures 10 through 13, these same computed fluxes are plotted against volume fraction of filler at discrete times.

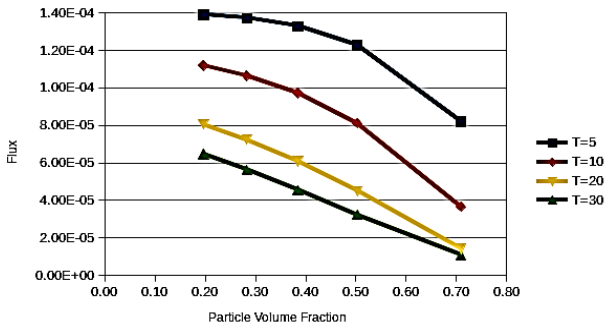

Figure 10. Flux at void interface plotted against volume fraction for the single particle model. Curves are plotted at discrete times of 5, 10, 20, and 30 seconds.

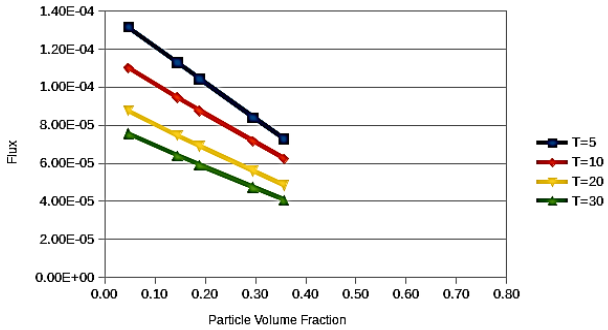

***Figure* 11.** Flux at void interface plotted against volume fraction for the two particle model. Curves are plotted at discrete times of 5, 10, 20, and 30 seconds.

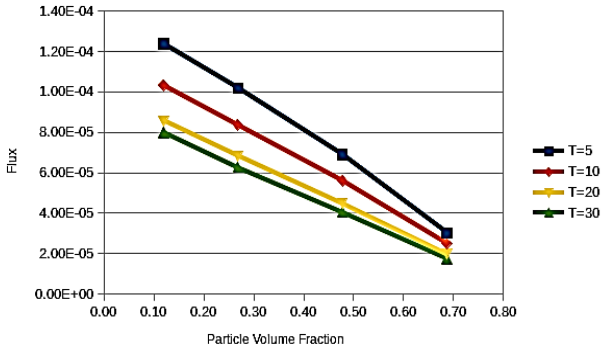

Figure 12. Flux at void interface plotted against volume fraction for the simple cubic lattice model. Curves are plotted at discrete times of 5, 10, 20, and 30 seconds.

Examination of these plots reveals that at moderate volume fractions, e.g. 0.20, the four models exhibit comparable flux values between 7.0e-5 and 6.0e-5 at time 30 seconds. At this longest time, the flux decreases linearly with increasing volume fraction in all four models as well. At time 5 seconds, the flux ranges between 1.4e-4 and 1.0e-4 at a volume fraction of 0.2, but unlike the linear behavior exhibited at time 30 seconds, the flux decreases at a rate that increases with increasing volume fraction.

Also, this nonlinear dependence on volume fraction varies among the four models, with the single particle model exhibiting the strongest nonlinearity and the two particle model the least.

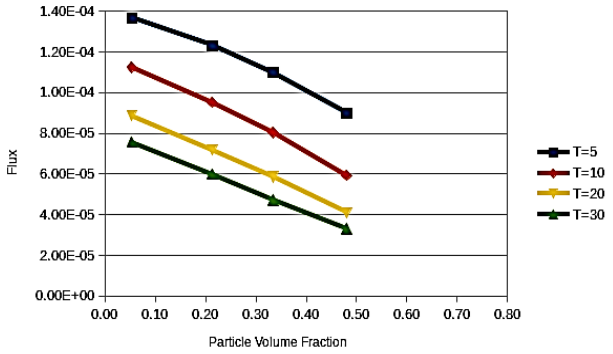

Figure 13. Flux at void interface plotted against volume fraction for the face centered cubic lattice model. Curves are plotted at discrete times of 5, 10, 20, and 30 seconds.

III. Test Introduction and Architecture

In addition to modeling, tests were performed in order to observe and understand void reduction from time zero onwards for a variety of applications. Tests were run on Armstrong's C7 (1:1 by weight) with varying adhesive cure temperatures (60-110°C) and volume fractions (0.30-.50). The filler used for testing was nickel coated hollow glass spheres that varied from 5-30um. The goal of testing was to observe void diffusion and reduction in the early stages of adhesive curing

For adhesive testing Armstrong's C7 was used. C7 has a variety of applications in electrically insulating applications. The 2 part epoxy can be mixed in different ratios depending on the application and can vary from hard to soft. C7 can also be cured over a variety of temperature ranges: room temperature for 1 week, or in heated environments in as little as a half an hour.

Based on the modeling, the highest flux values for all of the volume fractions are seen at the earliest time points of the adhesive curing. Tests were run to observe void formation and reduction at these early time points in the cure schedule. To determine test temperatures and cure states for C7 during these short test times, DSCs and TMAs were run. The glass transition temperature fell around 65°C Figure 14, and the adhesive at < 5 minutes of curing up to temperatures of 110°C would not see complete cure or hardening, Figure 15.

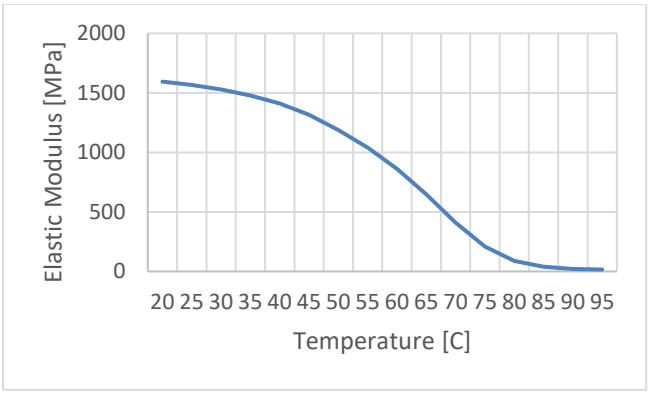

Figure 14. Elastic modulus of C7 as a function of temperature to determine the glass transition temperature.

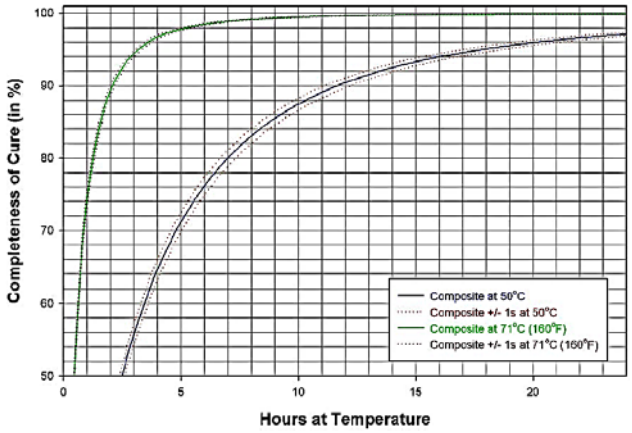

Figure 15. C7 extent of cure over the first 24 hours at 50°C and 71°C.

The C7 adhesive testing was performed using a microscope and hot plate to allow for real time data capture and observations. A 0.002" thick swatch of adhesive was placed onto glass slides to control the bondline thickness. The microscope slides were placed onto a hot plate beneath a microscope, Figure 16. Images were captured at 40X magnification for up to 5 minutes at 5 second intervals. The images were processed after the fact and observation notes were taken as the adhesive was heated. An example of the images taken are shown in Figure 17.

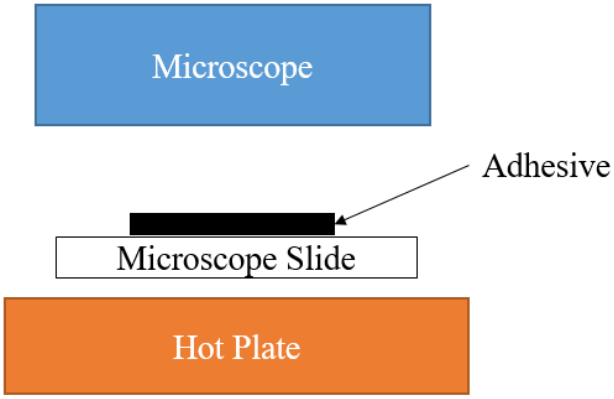

Figure 16. Image of the test architecture.

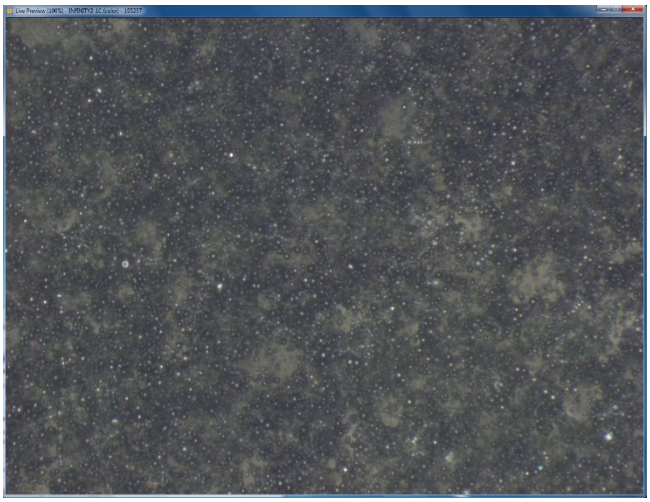

Figure 17. Example of images captured in the microscope. 100°C open face testing with 50% volume fraction.

To allow for flux diffusion, the testing was completed with an open face (glass slide on only one side of the adhesive). The filler chosen for testing were nickel coated glass spheres. C7 is a transparent adhesive, and the filler is a dark grey color. The dark grey spheres allowed for easier detection of voids, in comparison to using a transparent or white filler, Figure 18.

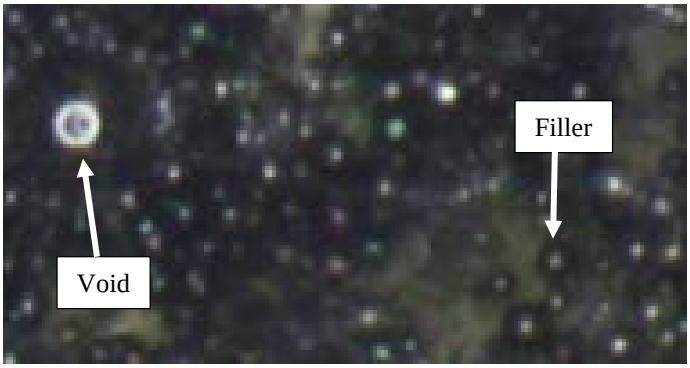

Figure 18. A zoomed in image of the 100°C 50% volume fraction image taken to show difference between void in microscope images and filler.

IV. Test Analysis and Summary

A variety of tests, Table 1, were run for 5 minutes and images were captured in 5 second intervals. Voids were tracked within the images, and the images were processed to determine void reduction over time.

Table 1. Test matrix

Set	Temperature (°C)	Volume Fraction
1	80	0.3 (30%)
2	80	0.5 (50%)
3	100	0.3 (30%)
4	100	0.5 (50%)
5	110	0.3 (30%)
6	110	0.5 (50%)

During testing, void reduction occurred rapidly. Rather than seeing a void reduce in size as time went on indicating gas diffusion into the C7, voids would fluctuate +/- 10% in diameter and then pop and dissipate over a 1s period at the exposed adhesive face.

Testing at 100°C or greater showed that there was a large increase in void reduction within the first 10 seconds of testing slide with the adhesive was placed on the hot plate, the existing voids experienced thermal shock from 25°C up to 100°C, which created increased gas diffusion from the voids into the air. When heating the voids to a lower thermal shock gradient (< 80°C) voids did not undergo rapid diffusion in the first 10 seconds.

Sets 1 and 2 showed no void reduction during the duration of the testing, however there were also no voids greater than 20um seen during the image processing. Sets 3 and 4 were the first times which we saw void reduction occur during testing. At 100°C, independent of the volume fraction, any observed voids between 20 and 40um in diameter saw a complete reduction in size within the first 30 seconds of testing. Sets 5 and 6 saw the

largest variation in results based on volume fractions. Set 5 showed over 90% of the void reduction occurred within the first 30 seconds of testing, whereas in set 6, over 60% of the void reduction occurred within the first 40 seconds of testing, and 50% within the first 30 seconds. Adhesive samples with smaller volume fraction experienced faster void reduction.

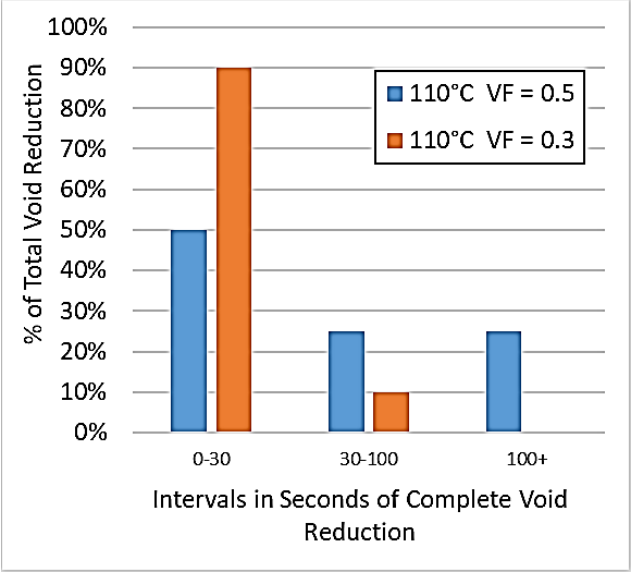

Figure 19. Comparison of time of complete void reduction as a function of time at 110°C at 30% and 50% volume fraction

Set 6 showed the largest range of void diameters seen within a single test. Set 6 showed voids with larger diameters tended to reduce faster than voids with smaller diameters, however there were cases in which small diameter voids also reduced quickly. For small diameter voids, reduction times were highly variable in the higher volume fraction condition. Some were reduced completed within the first 5 seconds of testing, and others took up to 190 seconds to reduce (Figure 20). The highly variable nature may indicate that with voids that are smaller than surrounding filler in higher volume fraction adhesives have a higher variability, and lower flux within the adhesive slows or inhibits void reduction.

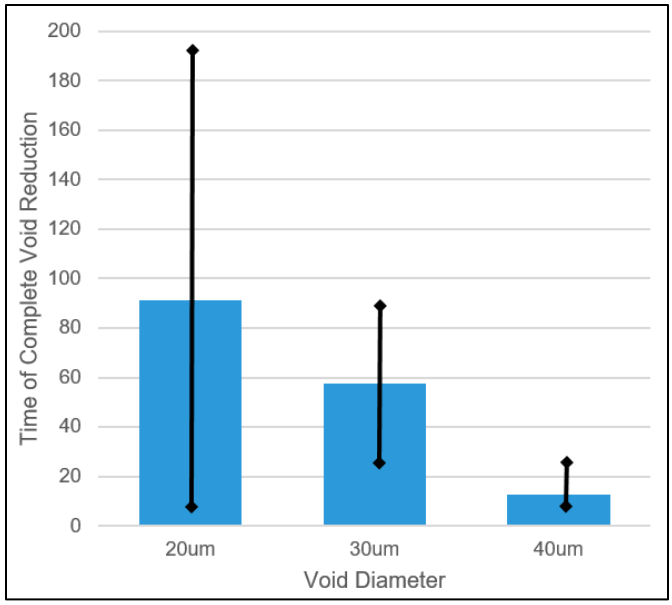

Figure 20. Comparison of time of complete void reduction as a function of void size at 110°C at 50% volume fraction

In lower volume fraction testing, the movement of filler was very prominent. From time zero, Figure 21, to 4 minutes, Figure 22, into testing, there was tendencies for the filler to congregate together, and leave other areas of the adhesive filler free. These trends were mostly seen in zero flux testing (microscope slides on both sides of the adhesive, and no face exposed to air). Although there was a trend of non-homogeneity, it only really became apparent after 30 seconds of heat exposure. Note that the images are both taken at 40X magnification.

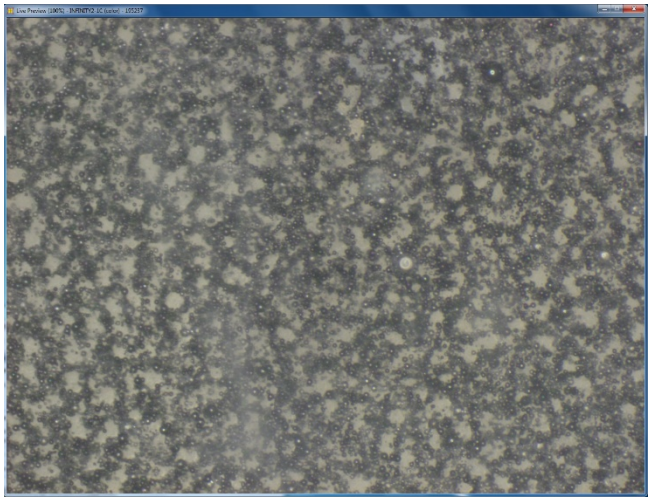

Figure 21. Filler placement for 80°C 30% volume fraction adhesive at time zero at 40X magnification. The darker areas indicate high filler presence areas, lighter areas are adhesive areas with less filler.

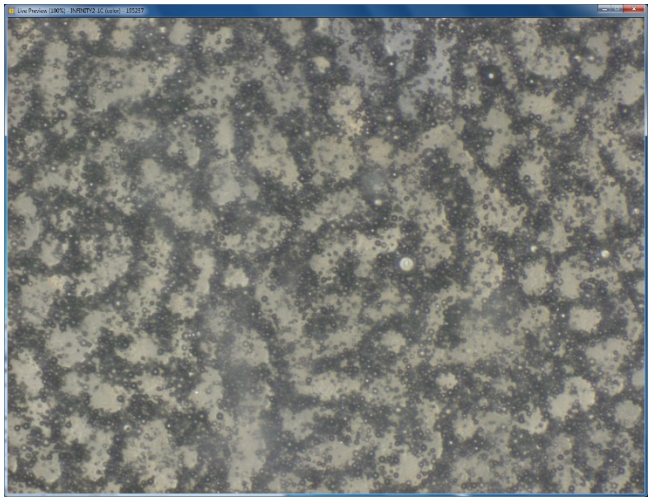

Figure 22. Filler placement for 80°C 30% volume fraction adhesive at time 2 minutes at 40X magnification. The darker areas indicate high filler presence areas, lighter areas are adhesive areas with less filler.

Adhesive joints with filler may be modeled as homogenous interfaces. When adhesive viscosity decreases the filler movement will increase; this may cause a homogenous adhesive at room temperature to become increasingly non-homogenous as the adhesive cross-links (but before it is completely cross-linked.) If adhesives are modeled as homogenous, however in micro-scale are really non-homogenous, there may be large disparities between model results and test results. An adhesive joint that has accumulation of filler in certain areas may see larger stress concentrations or varied thermal performance, which would cause failures earlier than anticipated in modeling efforts.

VIII. Conclusion

- Higher volume fraction adhesives have a lower flux which can prevent void reduction
- Flux at void interface drops quickly and by the same amount in all four particle models independent of particle volume fraction. This likely results from saturation of the adhesive in the immediate vicinity of the void.
- Time dependent decrease in flux is a strong function of particle volume fraction in all four particle models. This dependence is most pronounced in the two particle model. It is possible that the two different size particles block the diffusion field more efficiently than uniform size particles.
- At the longest times, all four particle models exhibit a linear dependence of flux on particle volume fraction.
- Use of lower volume fraction adhesives with heated cures may lead to increased non-homogeneity within the adhesive joints due to filler movement
- Void reduction was not seen in filled and closed face (microscope slide top and bottom) adhesive joints regardless of the temperature tested and volume fractions tested in this paper
- Use of high temperatures (110°C) for short durations (30 seconds) in the beginning of electronics assembly processes (prior to placing the second substrate on the adhesive) may remove voids without cross-linking or curing the adhesive

Acknowledgment

Thank you to Henry Raczkowski for his work on performing material characterization and providing data interpretation.

References

[1] Michael Hinchcliffe, Final Thesis Report, 2008, University of New South Wales, Australian Defense Force Academy, Canberra, Australia, “Characterization of Bond Line Porosity”

[2] Nina S. Dytiuk, Thomas F. Marinis, and Joseph W. Soucy, Proceedings IMAPS 2019, Boston, Massachusetts, “Control of Void Formation in Adhesively Bonded Joints”

[3] Nergizhan Kavac and Erhan Altan, Materials Science Forum, vol. 773-774, 2014, pp. 226-233, “Influence of Filler Amiunt and Content on the Mechanical Performance of Joints Bonded with Metal Powder Filled Adhesive”

[4] Diego P. M. Goncalves Antunes, Master’s Thesis, Aerospace Engineering, Tecnico Lisboa, 2015, “Understanding Failure of Adhesively Bonded Joints”

[5] R. J. Chester and J. D. Roberts, International Journal of Adhesion and Adhesives, vol. 9, no. 3, 1989, pp. 129-138, “Void Minimization in Adhesive Joints”

[6] “Elmer – Finite Element Solver for Multiphysical Problems,” http://www.csc.fi/elmer

[7] Christophe Geuzaine and Jean-Francois Remaele, International Journal for Numerical Metyhods in EZngineering, vol. 79, no. 11, 2009. Pp. 1309-1331, “Gmsh: a Three-Dimensional Finite Element Mesh Generator with Built-in Pre- and Post Processing Facilities”

[8] Utkarsh Ayachit**, The Para View Guide,** Kitware, 2020, available at http://paraview.org